NOTES AND CORRESPONDENCE

Life Cycle of a Linear Coastal-Trapped Disturbance

R. M. SAMELSON AND A. M. ROGERSON

Woods Hole Oceanographic Institution, Woods Hole, Massachusetts

27 October 1995 and 7 February 1996

ABSTRACT

A recent climatology of observed coastal-trapped disturbances in the marine atmospheric boundary layer along the United States west coast motivates the detailed examination, for a specific form of imposed forcing, of a linear shallow-water boundary layer model. The model is forced by a time-dependent pressure field, imposed at a fixed level above the boundary layer, that is an idealized representation of the climatological synoptic evolution: a low pressure center translates westward across the coastal boundary, corresponding to the observed offshore extension of a continental thermal trough. The alongshore structure of the model disturbance is characterized by enhanced northerly flow, a depressed marine layer, and low surface pressure to the north; and southerly flow, a raised marine layer, and high surface pressure to the south. Initially, the marine-layer thickness along the coast responds predominantly to convergence of the ageostrophic cross-shore flow driven by the imposed cross-shore pressure gradient and to convergence (to the south of the low pressure center) and divergence (to the north) of the geostrophic cross-shore flow balanced by the imposed alongshore pressure gradient, lifting in the central and southern parts of the forcing region and falling north of the forcing region. For the parameter values considered here, the amplitude of the coastal-trapped thickness response to the geostrophic cross-shore flow is roughly three times as large as that due to the ageostrophic cross-shore flow, but this ratio is likely to be sensitive to the cross-shore/alongshore aspect ratio of the pressure forcing. The coastal-trapped alongshore velocity disturbance is dominated by the response to the alongshore pressure gradient. There is no alongshore propagation in thickness disturbance during the initial stage of the event, while the alongshore velocity and surface pressure exhibit only weak propagation. In the later stages of the event, when the imposed coastal pressure gradients relax (as the low translates offshore), the cross-shore flow weakens, and the response at the coast is controlled by the convergence and divergence of the alongshore flow. The thickness disturbance, alongshore velocity reversal, and surface pressure perturbation propagate northward along the coast essentially as a Kelvin wave in the later stages of the event. Although both the model and the imposed pressure forcing are highly idealized, the model response is qualitatively and, to some degree, quantitatively consistent with many aspects of existing observations of coastal-trapped wind reversals along the United States west coast.

1. Introduction

Recently, Mass and Bond (1996) and Bond et al. (1996) have compiled a climatology of coastal-trapped wind reversals (Dorman 1985, 1987; Mass and Albright 1987) along the United States west coast. This climatology associates a specific synoptic and mesoscale evolution with the occurrence of the wind reversals, in which the western edge of a thermal trough that is normally resident over central California moves offshore in response to changes in the upper-level synoptic flow pattern, inducing a coastal-trapped response in the marine atmospheric boundary layer.

Rogerson and Samelson (1995) have formulated and analyzed a linear model of the coastal-trapped response of the marine atmospheric boundary layer to imposed changes in the pressure field just above the boundary layer. This model is similar in many respects to the models developed by Gill (1977) and Nguyen and Gill (1981) to investigate coastal-trapped lows along the coast of South Africa. In the present study, we reexamine the response of this model to forcing that is chosen to represent, in an idealized but specific manner, the pressure field found in the climatological analysis. We analyze the coastal-trapped response and the associated momentum and mass balances. Our goal is to provide a detailed description of the dynamics of this minimal model of a coastal-trapped disturbance, both to gain insight into the phenomena directly and for future comparison to observational data and more complex numerical simulations of specific observed events, in conjunction with the Coastal Meteorology Accelerated Research Initiative currently being sponsored by the Office of Naval Research (e.g., Ralph et al. 1995).

Corresponding author address: Dr. A. M. Rogerson, MS #21, Room 304A, Woods Hole Oceanographic Institution, Woods Hole, MA 02543.

2. Model formulation

a. Equations

The linear reduced-gravity shallow-water model of the marine atmospheric boundary layer used for the present calculations is described in detail by Rogerson and Samelson (1995). The model is forced by an imposed pressure field that is given at a fixed level above the boundary. The air–sea momentum flux (stress at the sea surface) is parameterized by a linearized drag law. A vertical wall represents the coastal mountain range, and a boundary condition of no normal flow is imposed along the wall. The disturbances generated by the interaction of the flow with the orographic lateral boundary are required to decay offshore.

The equations are

$$u_t + V_0 u_y - fv + \frac{p_x}{\rho} + \frac{ru}{H} = 0 \tag{1}$$

$$v_t + V_0 v_y + fu + \frac{p_y}{\rho} + \frac{rv}{H} = 0 \tag{2}$$

$$\zeta_t + V_0 \zeta_y + H(u_x + v_y) + \frac{w_* \zeta}{H} = 0, \tag{3}$$

where (u, v) are the horizontal velocities in the (x, y) directions (cross-shore and alongshore, respectively); t is time; p is surface pressure; ζ is the departure of the marine boundary layer thickness from the constant undisturbed value H; V_0 is a uniform alongshore velocity; f is the Coriolis parameter; ρ is the boundary layer air density; $g' = g\Delta\rho/\rho$ is the reduced gravity based on the density difference $\Delta\rho$ across the inversion; r is a linearized drag coefficient; w_* is a "diabatic velocity" damping coefficient; and subscripts x, y, t represent partial derivatives. (The diabatic damping is inserted in order that the Fourier transform solution may remain well posed in the limit of small frequency and alongshore wavenumber but has a negligible effect on the solution considered here.) The surface pressure p is composed of two parts,

$$p = p_a + g'\rho\zeta, \tag{4}$$

where p_a is the perturbation pressure forcing imposed at the fixed height $z = z_0$ above the marine layer (so $z_0 > H + \zeta$), and the second term in (4) is due to the deviation in marine layer thickness. {Note that the surface pressure p, as defined here, differs from the true surface pressure p_s by a dynamically irrelevant hydrostatic constant $p - p_s = -g[\rho z_0 - \Delta\rho(z_0 - H)]$ that is neglected because its gradient vanishes identically.} The wall representing the coastal orography is at $x = 0$, and the domain of the flow is west of the wall, $x < 0$. The boundary conditions are

$$u = 0 \quad \text{at} \quad x = 0 \tag{5}$$

and

$$u, v, \zeta \to 0 \quad \text{as} \quad x \to -\infty, \tag{6}$$

where the latter presumes that the pressure forcing also vanishes far from the coast. Solutions are obtained by Fourier transform, as described by Rogerson and Samelson (1995).

b. Forcing and parameter values

A specific synoptic evolution associated with warm-season coastal-trapped surface wind reversals along the United States west coast has been identified in the climatology of Mass and Bond (1996). At 850 mb and below, there is a strengthening and offshore extension of the thermal trough that is normally resident over the interior of southern California. The 850-mb height field evolution may be described as the westward propagation of a closed low pressure center above and across the coastal orography, at roughly 500 km day^{-1}. Such a description is particularly appropriate for the climatology of transitions at buoy 10 (Mass and Bond 1996, Fig. 3), located at the mouth of the Columbia River, near 46°N. The westward propagation continues for approximately two days before the low stalls offshore and weakens.

The pressure changes induced in the coastal marine atmospheric boundary layer by the synoptic and mesoscale evolution of the pressure field just above the top of the boundary layer will drive a coastal-trapped motion in the boundary layer. In the following calculation, we force the model boundary layer with a pressure distribution that approximately represents the structure of the climatological synoptic evolution at 850 mb, roughly a thousand meters above the mean inversion height. The alternative is to use a pressure forcing estimated from the climatological surface pressure evolution since no climatological information is currently available at intermediate levels. The present choice was made for two reasons. First, the surface pressure is affected by local changes in the boundary layer thickness, the prediction of which is the object of the present calculation. Second, the pressure evolution at 850 mb is relatively simple and easily represented and therefore intrinsically appropriate for use with the idealized model considered here. Nonetheless, it should be borne in mind that the synoptic and mesoscale evolution between 850 mb and the top of the boundary layer may result in a pressure forcing of the boundary layer whose detailed structure differs significantly from that of the 850-mb height field. In particular, it seems likely that lee troughing (e.g., Nuss 1995) may lead to a northward shift of the lower-level low pressure center relative to 850 mb and that the offshore extension of the lower-level thermal trough in the south may result in relatively weak lower-level alongshore pressure gradients south of the lower-level low pressure center.

In the following we analyze the response of the model to the imposed pressure forcing

$$p_a(x, y, t) = p_{a0}(x, y) + p_{a1}(x, y, t), \tag{7}$$

where the steady pressure field

$$p_{a0}(x, y) = \rho V_0\left(fx - \frac{ry}{H}\right) \quad (8)$$

geostrophically balances the uniform base-state velocity V_0, and the steadily propagating pressure pulse

$$p_{a1}(x, y, t) = Pe^{-\alpha[(x-Ut)^2+y^2]} \quad (9)$$

gives a first-order quantitative representation of the westward-propagating climatological low pressure center, with $P = -3$ mb, $U = -500$ km day^{-1}, and $\alpha = 8 \times 10^{-6}$ km^{-2}. The latter corresponds to a horizontal decay scale of 1000 km, purposely smaller than the smoothed feature appearing in the climatological mean. The center of the pulse crosses the coastal boundary $x = 0$ at the central latitude $y = 0$ at time $t = 0$. Note that a value of $-P$ as large as 5–6 mb could be consistent with the 850-mb height field, but since the model is linear in the disturbance from the base state, the response to the stronger forcing would differ only in disturbance amplitude. The representation (7)–(9) of the synoptic evolution is particularly appropriate for the 850-mb climatology at buoy 10, the northernmost buoy examined by Mass and Bond (1996), although a similar offshore extension of the continental thermal trough is associated with the transition at the other buoys. If the form of the pressure forcing were estimated instead from the climatological surface pressure field, instead of the 850-mb heights, a more asymmetric structure would be indicated, with weaker alongshore gradients to the south of the low pressure center. We discuss below the likely effect of such an asymmetry on the response. The isotropic form (9) does also appear to resemble closely the estimated surface pressure fields associated with certain coastal-trapped events, such as the strong May 1985 case analyzed by Mass and Albright (1987).

For the calculations described here, we fix the remaining parameters as follows: $H = 500$ m, $V_0 = -4$ m s^{-1}, $f = 10^{-4}$ s^{-1}, $\rho = 1.25$ kg m^{-3}, $g' = 0.3$ m s^{-2}, $r = 0.0075$ m s^{-1}, and $w_* = 0.001$ m s^{-1}. The relatively large value $H = 500$ m of the undisturbed marine-layer thickness was chosen in order to prevent the large thickness disturbances predicted by the linear model from exceeding the undisturbed thickness over a substantial portion of the domain. It results also in a relatively large linear Kelvin wave speed $c = (g'H)^{1/2} = 12$ m s^{-1}. In a nonlinear model, which properly represents the effects of finite-amplitude disturbances of the thickness, a smaller undisturbed (initial) thickness would probably be appropriate, and a similarly large nonlinear wave speed would arise in regions where the boundary layer thickness increases.

3. Results

The imposed low pressure pulse [Eq. (9)] crosses the coastline at $t = 0$, centered at the latitude $y = 0$ (Fig. 1a). The marine-layer thickness ζ responds initially by increasing near the coast at the central latitude and to the south and decreasing near the coast to the north (Fig. 1b). [Note that the magnitude of the marine layer thickness disturbance ζ reaches values comparable to the undisturbed thickness H, so that for forcing of the present amplitude, nonlinear effects (Dorman 1987; Hermann et al. 1990; Reason and Steyn 1992; Klemp et al. 1995) will generally be important. These effects are purposely neglected in the present study, the goal of which is to analyze in detail a minimal model of the coastal-trapped response.] The coastal marine-layer thickness disturbance develops near $y = 0$, $t = 0$ and then propagates northward as the pulse passes offshore and the forcing at the coast relaxes toward the base state. During the first day of northward propagation ($0 < t < 1$), the depression of the boundary layer north of $y = 0$ continues to increase in amplitude, while the coastal-trapped lifting to the south suffers a net decrease in amplitude. Offshore, the cross-shore velocity u that develops in the marine layer at $t = 0$ is directed onshore south of the central latitude and offshore to the north (Fig. 1c). The coastal-trapped response of alongshore velocity $v + V_0$ appears first as a wind reversal to southerly flow just south of the central latitude, which is evident by $t = 0$, and propagates northward, first growing, and then decaying, as the coastal forcing relaxes (Fig. 1d). A coastal-trapped intensification of the northerly flow develops at the northern edge of the pulse and propagates northward ahead of the reversal. Because the marine layer thickens rapidly along the coast beneath the southern part of the pulse, the lowest overall values of coastal surface pressure p are found to the north of the central latitude, and the surface low at the central latitude is located offshore (Fig. 1e, $t = 0$, $t = 1$).

As the imposed pressure pulse moves westward across the coast, pressure above the boundary layer at the coast falls 3 mb during the 36 h from $t = -1.5$ to $t = 0$ (where t is given in units of days) at the central latitude $y = 0$ and then returns to its undisturbed value during the following 36 h, from $t = 0$ to $t = 1.5$ (Fig. 2a). The coastal low pressure forcing weakens to the north and south, according to the imposed 1000-km horizontal scale. At the central latitude and to the south, the perturbation marine-layer thickness ζ at the coast increases during $-1 < t < 0$, roughly in proportion to the local strength of the forcing (Fig. 2b). To the north, and beginning 12 h later, the marine-layer thickness decreases, despite the local decrease in the imposed pressure above the boundary layer. During $-1 < t < 0$, there is little evidence of alongshore propagation of the coastal disturbance in marine-layer thickness. The thickness disturbances reach maximum amplitude near $t = 0.5$, half a day after the low pressure center crosses the coastal boundary, and then decay over the following 2 days. From $t = 0.5$ to t

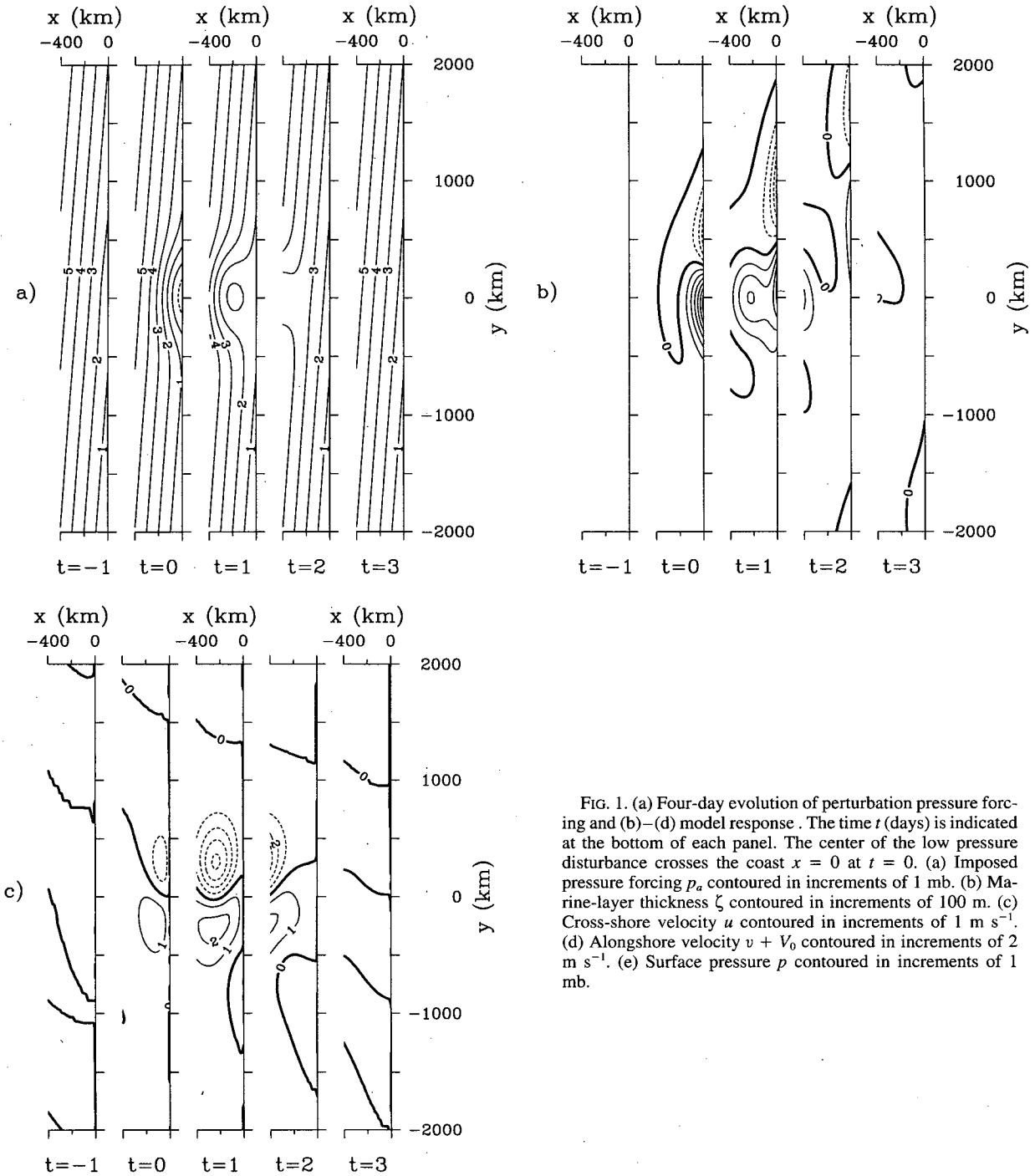

FIG. 1. (a) Four-day evolution of perturbation pressure forcing and (b)–(d) model response. The time t (days) is indicated at the bottom of each panel. The center of the low pressure disturbance crosses the coast $x = 0$ at $t = 0$. (a) Imposed pressure forcing p_a contoured in increments of 1 mb. (b) Marine-layer thickness ζ contoured in increments of 100 m. (c) Cross-shore velocity u contoured in increments of 1 m s^{-1}. (d) Alongshore velocity $v + V_0$ contoured in increments of 2 m s^{-1}. (e) Surface pressure p contoured in increments of 1 mb.

= 3, the maxima and zero crossing of the thickness disturbance propagate northward at a speed of approximately 700 km day^{-1}, roughly equal to the difference of the inviscid Kelvin wave speed $c = (g'H)^{1/2} = 12.25$ m s^{-1} and the 4 m s^{-1} southward base-state flow. The alongshore velocity $v + V_0$ and the surface pressure p {the sum of the imposed pressure forcing p_a and the pressure change due to the marine-layer thickness disturbance ζ [Eq. (4)]} also show evidence of propagation primarily after $t = 0$, when the low pressure center crosses the coast, with some evidence of weak propagation during $-1 < t < 0$ (Figs. 2c,d). North of the forcing region, all of the coastal disturbance fields have a propagating character. The cross-shore velocity u

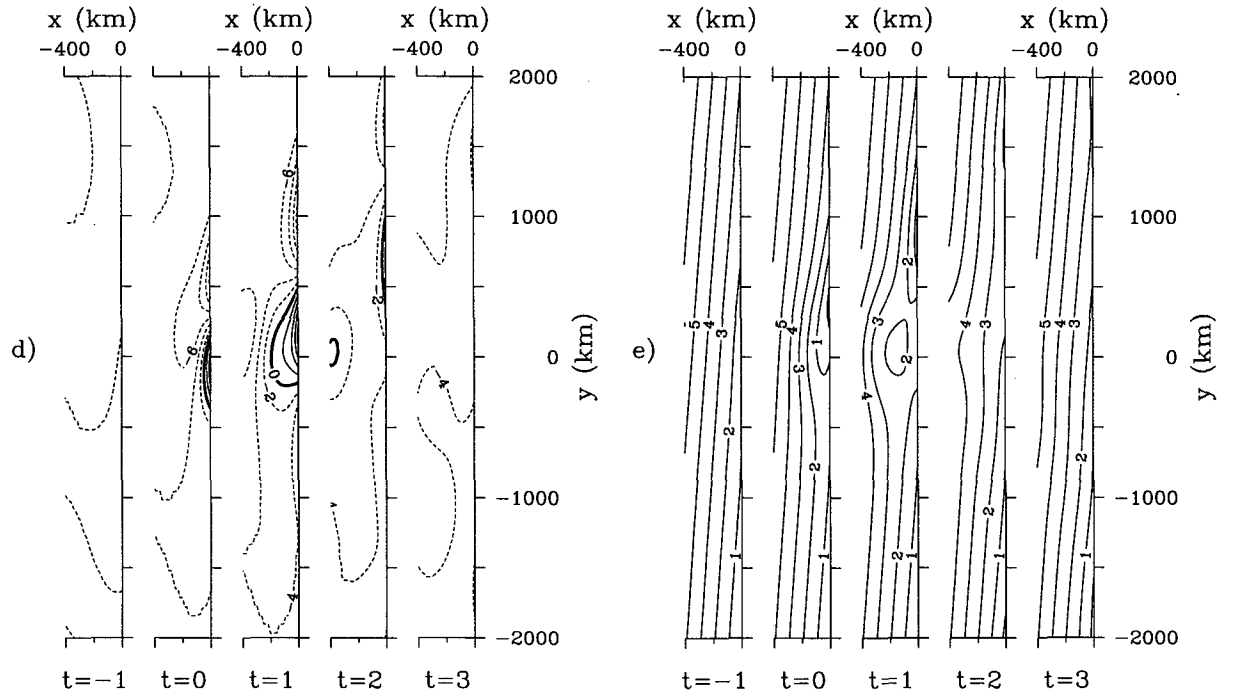

FIG. 1. (*Continued*)

at the coast vanishes identically, in accordance with the boundary condition [Eq. (5)].

Since the cross-shore velocity u vanishes at the coast, the cross-shore momentum balance there is exactly geostrophic: the Coriolis force due to the alongshore velocity $v + V_0$ balances the cross-shore gradient of the surface pressure p_x (Figs. 3a,b). The forcing p_a and the thickness ζ contribute differently to the total surface pressure. The forcing dominates initially and to the south, with the thickness gradient opposing the forcing gradient, while the thickness dominates to the north and after the forcing relaxes (Figs. 3c,d).

The vanishing of the cross-shore velocity also simplifies the alongshore momentum balance at the coast, since the corresponding Coriolis term vanishes, and the alongshore surface pressure gradient accelerates the alongshore flow directly against the surface drag (Figs. 4a–d). The local acceleration of the alongshore flow (Fig. 4a) and the surface pressure gradient (Fig. 4d) propagate northward at roughly the linear Kelvin wave speed, relative to the southward base flow, while the alongshore pressure gradient due to the marine-layer thickness gradient has a propagating character only in the later stages of the event (Fig. 4f). The linearized momentum advection $V_0 v_y$ is comparable to the local acceleration v_t during the entire event (Figs. 4a,b).

Although the cross-shore velocity u vanishes at the coast, its divergence u_x does not, and the marine-layer thickness deviation ζ evolves in response to convergence and divergence of both cross-shore and alongshore flow, along with thickness advection by the base-state velocity field (Fig. 5). During the initial stage of the event ($-1 < t < 0$), the thickness responds primarily to the cross-shore convergence and divergence (Fig. 5c), as the alongshore thickness advection roughly balances the alongshore convergence and divergence (Figs. 5b,d). Consequently, the thickness increases in the southern part of the forcing region but decreases to the north, despite the local decrease in pressure above the boundary layer in the northern part of the forcing region (Fig. 2b). During the later stages of the event ($t > 0.5$), the magnitude of the divergence of the cross-shore flow weakens rapidly, and the thickness is controlled primarily by the convergence and divergence of the alongshore flow (Fig. 5d). The transition between the two dynamical stages of the event at the coast is marked by a change in sign of the marine-layer thickness tendency ζ_t that occurs near $t = 0.25$, roughly 6 h after the low pressure center crosses the coast (Fig. 5a).

The momentum balances described above are superficially similar to those for a Kelvin wave disturbance during the entire event, if only the total surface pressure is considered, and not its separate contributions from the forcing and the thickness disturbance. However, the thickness evolves according to the Kelvin wave mass balance only in the later stages of the event, when the forcing has relaxed. During the initial stage of the event, when the local forcing is greatest, the cross-shore divergence (which vanishes identically every-

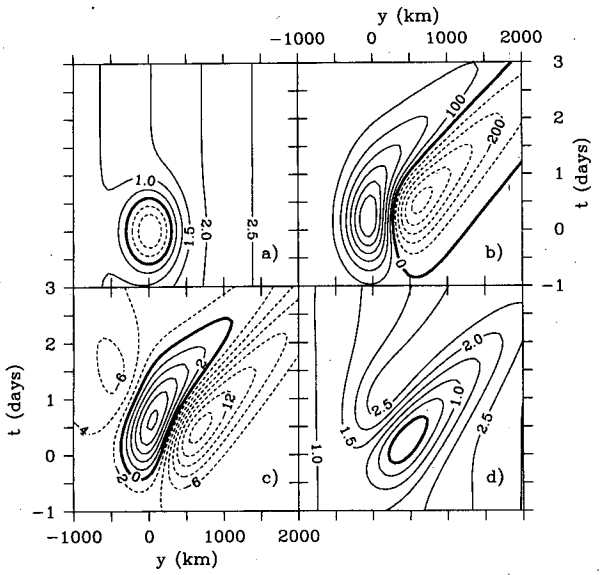

FIG. 2. (a) Coastal pressure forcing and (b)–(d) model response as functions of alongshore distance and time. (a) Imposed pressure forcing p_a contoured in increments of 0.5 mb. (b) Marine-layer thickness ζ contoured in increments of 100 m. (c) Alongshore velocity $v + V_0$ contoured in increments of 2 m s^{-1}. (d) Surface pressure p contoured in increments of 0.5 mb.

where for a Kelvin wave) controls the evolution of the coastal marine-layer thickness. The different roles of the convergence and divergence of cross-shore and alongshore flow and the different effects of the imposed cross-shore and alongshore pressure gradient forcing may be illustrated with two approximate solutions to the Eqs. (1)–(4). These approximate solutions, derived below by approximating the equations of motion, may also be obtained by corresponding approximations to the Fourier transform solution of Eqs. (1)–(4) given by Rogerson and Samelson (1995), following the residue calculation for forced oceanic Kelvin waves presented by Thomson (1970) and using (for example) an exponential function of distance rather than distance squared for the pressure forcing to facilitate the residue computation. In order to derive these solutions, it is convenient first to assume that the damping coefficients for height and velocity are equal, so that

$$\frac{r}{H} = \frac{w_*}{H} = r_0. \tag{10}$$

Here r_0 is the inverse of a generalized damping timescale of the disturbance, for which a value of roughly 3 days yields solutions that are generally similar to those obtained for the values of r and w_* used above.

If the cross-shore pressure gradient forcing dominates the alongshore gradient, as might be expected to occur near $y = 0$ when the low pressure pulse first impinges on the coast, or more generally if the cross-shore scale of the pulse is relatively short, then all the alongshore gradients should be negligible, and Eq. (1)–(4) may be approximated by

$$u_t + r_0 u - fv = -g'\zeta_x - P'_x \tag{11}$$

$$v_t + r_0 v + fu = 0 \tag{12}$$

$$\zeta_t + r_0\zeta + Hu_x = 0, \tag{13}$$

where $P' = P/\rho$. From these three equations, a single equation may be derived for the cross-shore flow u,

$$u_{tt} + 2r_0 u_t + r_0^2 u + f^2 u - c^2 u_{xx} = -(P'_{xt} + r_0 P'_x). \tag{14}$$

Under the additional assumptions that u_{tt}, $r_0 u_t$, $r_0^2 u \ll f^2 u$ (that is, the local and frictional timescales of u are small compared to f^{-1}), and that P'_x may be approximated by its value at $x = 0$ (so the offshore scale of the disturbance is small relative to the offshore scale on which the pressure gradient changes), these equations have the solution

$$u = -f^{-2}(P'_{xt} + r_0 P'_x)(1 - e^{\gamma x}) \tag{15}$$

$$v = f^{-1}(1 - e^{\gamma x})e^{-rt}\int_{-\infty}^{t} e^{rt'}(P'_{xt'} + r_0 P'_x)dt' \tag{16}$$

$$\zeta = -(g'\gamma)^{-1}P'_x e^{\gamma x}, \tag{17}$$

where $\gamma = f/c$ is the inverse of the boundary layer deformation radius. Thus, there is a "quasi-static" coastal-trapped deformation of the boundary layer that

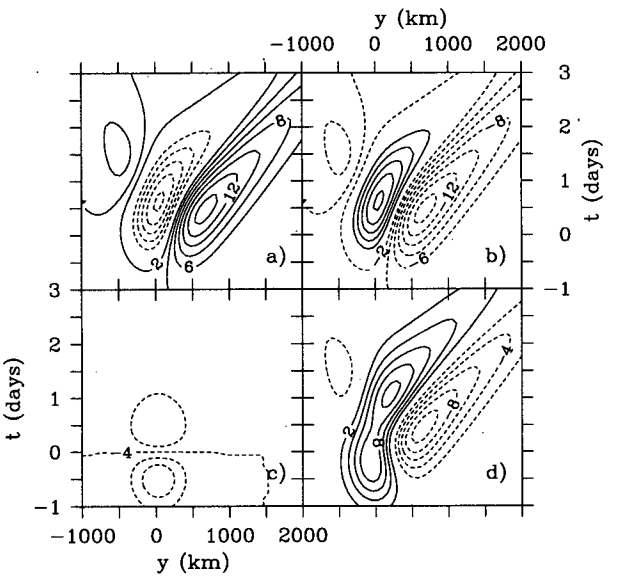

FIG. 3. Cross-shore momentum balance at the coast in units of 10^{-4} m s^{-2}. The contour increment is 2×10^{-4} m s^{-2}. (a) Coriolis term $-f(v + V_0)$. (b) Surface pressure gradient p_x/ρ. (c) Forcing contribution to surface pressure gradient p_{ax}/ρ. The unlabeled contours appearing for $t < 0$ are -6 and -8×10^{-4} m s^{-2}, and that for $t > 0$ is -2×10^{-4} m s^{-2}. (d) Layer thickness contribution to surface pressure gradient $g'\zeta_x$.

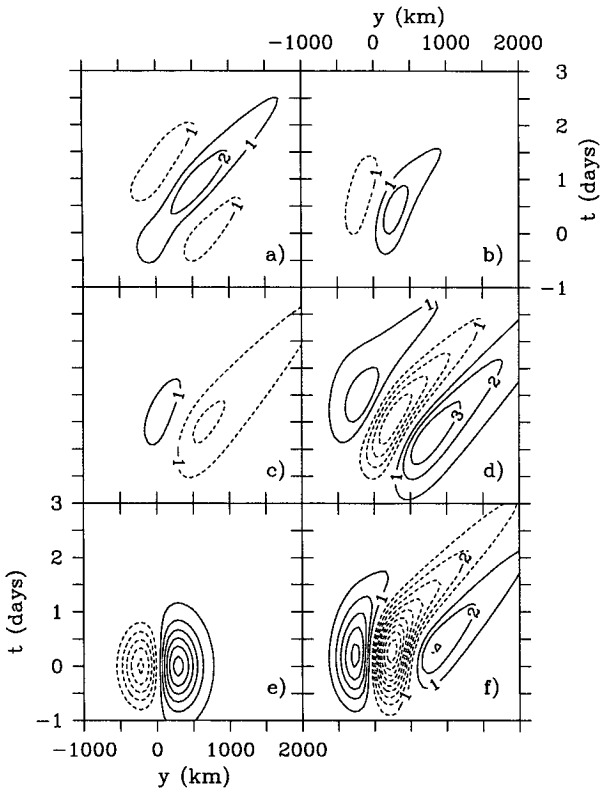

FIG. 4. Alongshore momentum balance at the coast in units of 10^{-4} m s^{-2}. The contour increment is 1×10^{-4} m s^{-2}. (a) Local acceleration v_t. (b) Advective acceleration $V_0 v_y$. (c) Surface drag $(r/H)(v + V_0)$. (d) Surface pressure gradient p_y/ρ. (e) Forcing contribution to surface pressure gradient p_{ay}/ρ. (f) Layer thickness contribution to surface pressure gradient $g'\zeta_y$.

is locally proportional to the instantaneous cross-shore pressure gradient forcing (in the low-frequency limit, that is, neglecting adjustment on timescales comparable to f^{-1}). The vanishing of the cross-shore velocity at the coast ($x = 0$) requires such a response in order to satisfy the cross-shore momentum balance (11) at the coast, since in the absence of alongshore pressure gradients no alongshore velocity (which might otherwise balance the pressure gradient geostrophically) can then be generated at the coast, because the alongshore momentum balance (12) is inertial. The necessary divergence is supplied by the ageostrophic offshore flow, which far from the coast inertially balances the acceleration of the alongshore flow, which in turn is able far from the coast to balance the cross-shore pressure gradient geostrophically.

If the alongshore pressure gradient forcing dominates the cross-shore gradient, and if the rate of change (and frictional drag) of the cross-shore flow is small relative to the alongshore flow, as might be expected to occur near $t = 0$, when the cross-shore pressure gradient forcing vanishes, the cross-shore momentum equation may be replaced by a condition of geostrophic balance, and a form of the semigeostrophic equations results:

$$-fv = -g'\zeta_x \tag{18}$$

$$v_t + V_0 v_y + r_0 v + fu = -g'\zeta_y - P'_y \tag{19}$$

$$\zeta_t + V_0\zeta_y + r_0\zeta + H(u_x + v_y) = 0. \tag{20}$$

The latter two equations may be rewritten

$$g'(\zeta_t + V_0\zeta_y + r_0\zeta)_x + f^2 u_a = 0 \tag{21}$$

$$\zeta_t + V_0\zeta_y + r_0\zeta + Hu_{ax} = 0, \tag{22}$$

where the ageostrophic cross-shore velocity is $u_a = u - u_g$, $u_g = -g'\zeta_y/f - P'_y/f$, and again the forcing pressure gradient (P'_y) is approximated by its value at $x = 0$. Either of u_a or ζ may then be eliminated to yield an equation in the other that may be readily solved, with the boundary condition $u_a(x = 0) = -u_g(x = 0)$. Substitution of the result into either of the last two equations above yields the equations

$$u = -f^{-1}P'_y(1 - e^{\gamma x}) \tag{23}$$

$$v = cH^{-1}D(y, t)e^{\gamma x} \tag{24}$$

$$\zeta = D(y, t)e^{\gamma x}, \tag{25}$$

where the amplitude $D(y, t)$ of the coastal-trapped deformation of the boundary layer satisfies the 1D wave equation

$$D_t + V_0 D_y + r_0 D + cD_y = -Hc^{-1}P'_y. \tag{26}$$

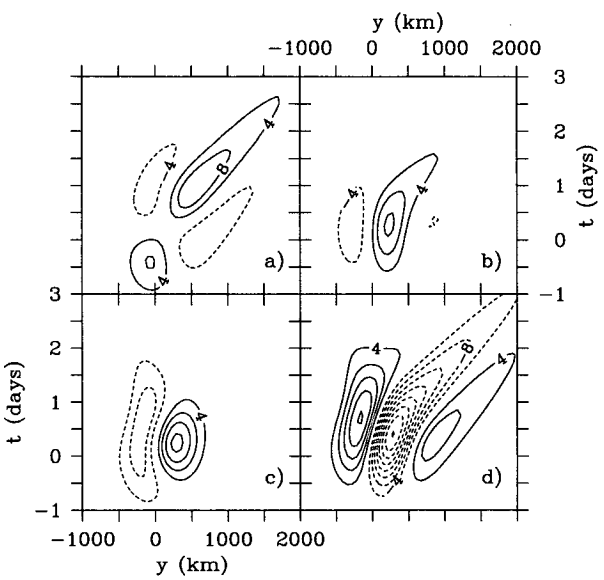

FIG. 5. Mass balance at the coast in units of 10^{-3} m s^{-1}. The contour increment is 4×10^{-3} m s^{-1}. (a) Local thickness change ζ_t. (b) Thickness advection $V_0\zeta_y$. (c) Divergence of cross-shore flow Hu_x. (d) Divergence of alongshore flow Hv_y.

The latter may be easily solved numerically (or analytically, in terms of error functions for the analytic form of the forcing assumed here). This approximation is the basis of related work on coastal lows by Gill (1977) and Nguyen and Gill (1981). A similar approximate system of equations for coastal-trapped disturbances, with forcing from an imposed distribution of vertical velocity at the top of the boundary layer instead of an imposed pressure gradient as here, has been discussed previously by Reason and Steyn (1990). The wave equation (26) allows an interpretation of the continuity equation, in which the first three terms are the damped rate of change of ζ, the fourth is the divergence of the alongshore flow (Hv_y), and the right-hand side is the convergence of the cross-shore flow ($-Hu_x$), with each term decaying exponentially over the offshore scale c/f. Thus, the cross-shore convergence (which is proportional to the local forcing and has no resonant structure) affects the coastal boundary layer thickness solely as a local forcing, while the alongshore convergence is entirely an intrinsic part of the wave dynamics. In conjunction with the solution for the cross-shore velocity u, it also allows an interpretation of the alongshore momentum equation, in which there is a smooth (exponential) transition over the cross-shore scale c/f from geostrophic balance ($fu = -p_y/\rho$) offshore to downgradient acceleration ($v_t + r_0 v = -p_y/\rho$) at the coast.

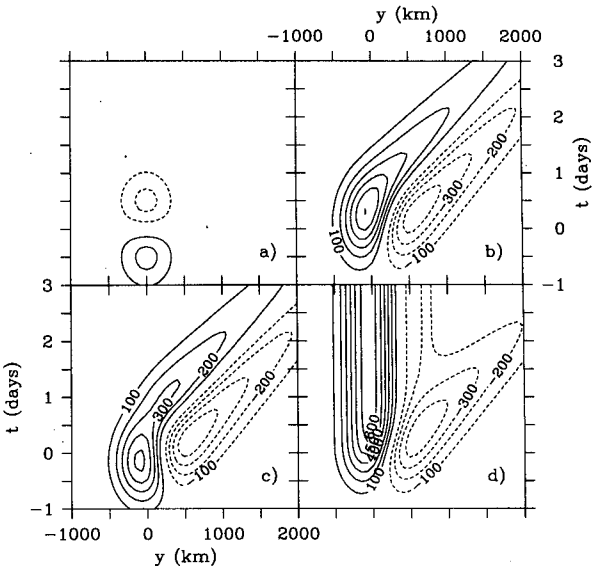

FIG. 6. Marine-layer thickness ζ at the coast from the approximate solutions, contoured as a function of alongshore distance and time, in increments of 100 m. (a) The quasi-static response. (b) The Kelvin wave response. (c) The sum of the quasi-static and Kelvin wave responses. (d) The Kelvin wave response for the case in which the forcing propagation halts at $t = 0$.

These two sets of approximate solutions provide a useful quantitative and conceptual decomposition of the Fourier transform solution. The quasi-static coastal-trapped response to the cross-shore pressure gradient forcing has a maximum amplitude of roughly 200 m (Fig. 6a) and has no propagating character. The forced Kelvin wave response reaches an amplitude of 600 m near $t = 0.5$, with only weak propagation for $t < 0$, and then propagates northward as a damped free Kelvin wave (Fig. 6b). The sum of the two solutions (Fig. 6c) is close to the transform solution (Fig. 2b), with differences due to the different dissipation coefficients, the dynamical approximations, and the approximation of the pressure gradient forcing near the coastal boundary. The structure of the transform solution for $v(x = 0; y, t)$ resembles the wave-equation approximate solution alone, since the alongshore velocity disturbance (v) at the coast is proportional to ζ in the wave-equation solution, but vanishes identically in the quasi-static solution. The importance of the quasi-static balance in the cross-shore momentum equation at the coast in the transform solution is evident from the compensation of the thickness and forcing pressure gradients (Fig. 3).

Although the detailed structure of the climatological synoptic or mesoscale low pressure forcing associated with the observed coastal-trapped wind reversals is uncertain, a westward propagation of the imposed low pressure pulse that halts at the coast at $t = 0$ may be more representative of the observations than the continued offshore propagation for $t > 0$ assumed here, while the latter is required in order that the response may be conveniently analyzed using the solutions obtained by Rogerson and Samelson (1995). An approximate solution in the former case may, however, be easily obtained from the equations derived above. The quasi-static solution is fixed to the local value of the cross-shore pressure gradient, so the steady response to the cross-shore pressure gradient is (in that approximation) equal to the instantaneous response. At $t = 0$, the imposed cross-shore pressure gradient vanishes, so the quasi-static response also vanishes. The solution of the wave equation (26) for the case in which the low pressure pulse propagation halts at $t = 0$ shows that the response separates into two parts, a local steady response to the fixed forcing, and a northward-propagating damped wave response to the time-dependent forcing during $t < 0$ (Fig. 6d). For the wave equation, as noted above, the coastal-trapped alongshore velocity disturbance is directly proportional to the thickness disturbance.

As noted above, the form of the pressure forcing used here may overestimate the strength of the alongshore pressure gradient south of the low pressure center. The approximate solutions suggest that the quasi-static response to the cross-shore pressure gradient will, at least initially, dominate the southern response in that case. Since the Kelvin wave dynamics lead to a response to the integrated alongshore pressure gradient, the later response may still be dominated by the forced Kelvin wave. This will depend on the damping, the wave speed, and the detailed structure of the forcing.

4. Discussion

The results summarized above describe the response of the linear model to pressure forcing chosen to represent the climatological synoptic evolution that has been associated with coastal-trapped wind reversals by Mass and Bond (1996). These results may be compared to the climatological characterization of the structure and evolution of coastal-trapped wind reversals that has been compiled and described by Bond et al. (1996).

The observed wind reversals have timescales of 24–36 h, alongshore scales of 500–1000 km, and wind speed changes of 10–20 m s^{-1} and are accompanied by surface pressure changes of 4–8 mb (Bond et al. 1996). The results from the linear theory are generally comparable to these values, except for the predicted changes in surface pressure, which are a factor of two smaller than observed changes. The temporal evolution of the model disturbance is also in general accord with the observations. At a fixed coastal location, the observed pressure minimum typically occurs a few hours before the wind reversal. The predicted pressure minimum similarly occurs a few hours before the wind reversal near the central latitude $y = 0$, where maximum southerly flow is found in the model; farther north, the predicted wind reversal occurs progressively later relative to the local pressure minimum, while the surface pressure is rising. The smooth reversal in the model is qualitatively similar to the reversals observed at the southern buoys and noticeably different from the abrupt reversals observed at the northern buoy (buoy 10), in which the transition to southerly flow is achieved in 2–3 h.

The alongshore structure of the model disturbance is characterized by enhanced northerly flow, a depressed marine layer, and low surface pressure to the north, and southerly flow, a raised marine layer, and high surface pressure to the south. Direct measurements of the marine-layer thickness were not available for the climatological analysis, but the observed transitions to southerly flow were generally accompanied by a similar reversal in the alongshore pressure gradient (Bond et al. 1996). There was only a weak indication of enhanced northerly flow during the 24–36 h prior to the wind reversal for the observed transitions at buoy 13 (located northwest of San Francisco Bay) and no such indication at the other buoys. This discrepancy is likely due primarily to two shortcomings of the linear theory: the linear model predicts severe thinning and eventual vanishing of the boundary layer in the region of enhanced northerly flow and so is formally invalid there, and in addition the linear parameterization of the vertical turbulent stress divergence is inaccurate in this region since it neglects the change in boundary layer thickness. Previous dynamical modeling of northerly flow in the coastal marine atmospheric boundary layer along the United States west coast has emphasized the role of enhanced deceleration by surface drag in shallow parts of the boundary layer (Samelson 1992).

The climatological analysis indicates that the observed wind reversals propagate northward at 7–8 m s^{-1} north of buoy 13 but show no significant propagation south of buoy 13 (Bond et al. 1996). Since the central latitude of the offshore extension of the continental thermal trough (presumed in the present model to generate the coastal-trapped disturbances) is generally located at buoy 13 or farther south, this geographic division of the disturbance into nonpropagating (southern) and propagating (northern) regimes is evidently consistent with the similar division of the model disturbance regimes relative to the latitude of the imposed pressure forcing. To the extent that the thermal troughs move north of buoy 13, which can occur, this conclusion does not follow. With reference to the approximate solutions discussed above, buoy 13 may represent the alongshore location where the integrated, propagating response to the alongshore pressure gradient exceeds the local response to the cross-shore pressure gradient in the climatological mean. The agreement of the linear model propagation speed with the observed value would be degraded if a smaller (and probably more realistic) value of undisturbed boundary layer thickness were used in the model, consistent with the possibility that nonlinearity (Dorman 1987; Hermann et al. 1990; Reason and Steyn 1992; Klemp et al. 1995) enhances the northward propagation speed of the observed disturbances.

The model results described above emphasize the importance of convergent (onshore) and divergent (offshore) cross-shore boundary layer flow, which control the evolution of the boundary layer thickness either locally or in conjunction with the Kelvin wave dynamics of the alongshore flow. This convergent and divergent motion is the consequence of the geostrophic adjustment of flow in the offshore boundary layer to changes in the synoptic pressure gradient. The approximate solutions illustrate that the coastal disturbance in boundary layer thickness that arises in response to this motion has essentially two components: a local (in y and t) response to the cross-shore pressure gradient and a Kelvin wave response to the alongshore pressure gradient. The Kelvin wave component of the rate of change of the coastal thickness may be further decomposed into a response to the local cross-shore convergence (Hu_x) and a response to the local alongshore convergence (Hv_y) that is itself an integrated response to the cross-shore convergence encountered previously along the wave characteristics $q = y - ct$. In this respect, our results are consistent with the hypothesis (Dorman 1985; Reason and Steyn 1990; Klemp et al. 1995) that convergent onshore flow in the boundary layer might initiate a coastal-trapped disturbance by locally thickening the boundary layer near the coast but show additionally that the responses to cross-shore flow driven by cross-shore and alongshore pressure gradi-

ents are dynamically distinct. Note that the large amplitude of the model marine-layer thickness disturbance may exaggerate the thickness contribution to the boundary layer pressure gradient in the later stages of the present calculations and thus exaggerate the relative importance of the Kelvin wave dynamics, and also that the imposed pressure field may exaggerate the alongshore pressure gradients (and thus the geostrophic onshore flow) south of the low-pressure center.

The occurrence of offshore flow in the north, associated with the extension of the east Pacific high into southwest Canada and the Pacific Northwest, is an important aspect of the climatology presented by Mass and Bond (1996): the offshore flow produces a strengthening and offshore extension of an interior thermal trough (by lee troughing or warm advection, or both), reversing the alongshore pressure gradient and ageostrophically accelerating southerly flow. It is important to emphasize that this climatological synoptic or mesoscale offshore flow, which occurs above the boundary layer, differs fundamentally from the divergent offshore flow in the boundary layer that occurs in the model, which is a response to the pressure forcing imposed (effectively) just above the top of the boundary layer. If lee troughing (Mass and Albright 1987; Nuss 1995) does significantly alter the synoptic pressure field, then the low pressure center just above the boundary layer should occur beneath the strongest lower-level offshore flow, 500–1000 km to the north of the center of the closed low in the 850-mb height field. The strongest southerly flow in the model was found near the central latitude of the forcing; in contrast, the climatology, which is presumably dominated at each buoy by events that peak at or near that buoy, places the center of the 850-mb trough 500–1000 km south of the buoy at which the reversal was observed. The mechanism of lee troughing and the associated northward shift of the near-surface low pressure center relative to the 850-mb trough might partially reconcile this apparent discrepancy.

Recent analysis of observations of a June 1994 event (Ralph et al. 1995) reveal some features that are consistent with the model results (e.g., Fig. 1). A narrow mesoscale coastal ridge was observed, with pressure decreasing to the north. Southerly flow was found under the ridge, with maximum northerly flow approximately 600 km to the north. A mesoscale low located 200 km offshore, adjacent to the coastal ridge, was also observed, coincident with low wind speeds. Offshore flow preceded the wind reversal in the central and northern part of the disturbance. A similar mesoscale pressure pattern associated with a coastal-trapped wind reversal was observed previously by Mass and Albright (1987). Other aspects of the June 1994 event are not well represented by the linear shallow-water model. For example, the vertical structure of the observed disturbance evidently was dominated by changes in the structure of the thick inversion capping the marine boundary layer, not simply by changes in the thickness of the boundary layer (Ralph et al. 1995).

5. Summary

We have considered the linear adiabatic coastal-trapped response of a stable coastal marine atmospheric boundary layer to forcing representative of the climatological synoptic evolution associated with observed coastal-trapped wind reversals. The results indicate that the response occurs in two stages and that the dynamics controlling the response to the cross-shore and alongshore pressure gradients are distinct. Far from the coast, an alongshore flow develops that is in geostrophic balance with the imposed cross-shore pressure gradient; the acceleration of this geostrophic flow is inertially balanced with an ageostrophic cross-shore flow, and the coastal boundary layer thickness responds directly to the convergence or divergence of this ageostrophic cross-shore flow. For the parameters considered here, this response has an amplitude of roughly 200 m, and, to first order, there is no accompanying response of the alongshore winds at the coast. In contrast, the imposed alongshore pressure gradient does force (geostrophic) alongshore flow at the coast, as the coastal thickness and alongshore velocity response are together described by forced Kelvin wave dynamics. A cross-shore flow far from the coast develops that is in geostrophic balance with the alongshore pressure gradient, and the convergence and divergence of this flow provide the forcing for the Kelvin wave. For the parameters considered here, this response has an amplitude of roughly 600 m. The ageostrophic response to the alongshore pressure gradient is limited to a cross-shore flow that is equal and opposite to the geostrophic cross-shore flow at the coast and decays offshore on the scale of the internal deformation radius of the boundary layer.

The superposition of these two effects, and the forced Kelvin wave response itself, lead to a coastal-trapped response that occurs essentially in two stages. Initially, the marine layer lifts along the coast in response to convergence of the ageostrophic onshore flow, and (half a day later) lifts to the south and falls to the north of the low pressure center in response to the convergence and divergence of the geostrophic cross-shore flow. Thus, in this first phase of "generation" of the disturbance, the boundary layer thickens more rapidly to the south of the low pressure center than to the north, and this asymmetry is amplified by the Kelvin wave dynamics associated with the alongshore flow at the coast. Subsequently, as the forcing relaxes, the offshore and onshore flows weaken, and the thickness evolution at the coast during this second "propagation and decay" phase, is controlled by the convergence and divergence of the alongshore flow. The ageostrophic cross-shore flow during the latter stage depends on the character of the imposed cross-shore pressure gradient, which may not be well mod-

eled by the steady westward propagation of the low pressure center in the present calculation. The disturbance resembles a free Kelvin wave more closely during the latter stage.

The detailed structure of the synoptic or mesoscale low pressure disturbances associated with the coastal-trapped wind reversals remains uncertain, and the details of any specific event will differ in some measure from the climatological mean (e.g., Ralph et al. 1995). In addition, it is clear that nonlinear and diabatic effects, among others, must influence the generation, propagation, and decay of the coastal-trapped response. Nonetheless, the linear model presented here is qualitatively and, to some degree, quantitatively consistent with many aspects of existing observations of coastal-trapped wind reversals along the United States west coast.

Acknowledgments. The present calculation was partially stimulated by a comment from M. Ralph. This research was supported by the Office of Naval Research, Grants N00014-92-J-1589 and N00014-93-1-1369, code 322MM, and Contribution 9132 from the Woods Hole Oceanographic Institution.

REFERENCES

Bond, N., C. Mass, and J. Overland, 1996: Coastally trapped wind reversals along the United States west coast during the warm season. Part I: Climatology and temporal evolution. *Mon. Wea. Rev.*, **124,** 430–445.

Dorman, C. E., 1985: Evidence of Kelvin waves in California's marine layer and related eddy generation. *Mon. Wea. Rev.*, **113,** 827–839.

——, 1987: Possible role of gravity currents in northern California's coastal summer wind reversals. *J. Geophys. Res.*, **92,** 1497–1506.

Gill, A. E., 1977: Coastally trapped waves in the atmosphere. *Quart. J. Roy. Meteor. Soc.*, **103,** 431–440.

Hermann, A. J., B. M. Hickey, C. F. Mass, and M. D. Albright, 1990: Orographically trapped coastal wind events in the Pacific Northwest and their oceanic response. *J. Geophys. Res.*, **95,** 13 169–13 193.

Klemp, J., R. Rotunno, and W. Skamarock, 1995: Shallow-water model simulations of coastally trapped disturbances. *Proc. of the Seventh Conf. on Mountain Meteorology,* Breckenridge, CO, Amer. Meteor. Soc., 197–202.

Mass, C. F., and M. D. Albright, 1987: Coastal southerlies and alongshore surges of the west coast of North America: Evidence of mesoscale topographically trapped response to synoptic forcing. *Mon. Wea. Rev.*, **115,** 1707–1738.

——, and N. Bond, 1996: Coastally trapped wind reversals along the United States west coast during the warm season. Part II: Synoptic evolution. *Mon. Wea. Rev.*, **124,** 446–461.

Nguyen, N. A., and A. E. Gill, 1981: Generation of coastal lows by synoptic-scale waves. *Quart. J. Roy. Meteor. Soc.*, **107,** 521–530.

Nuss, W., 1995: Lee troughing and the evolution of a coastally trapped disturbance. *Proc. of the Seventh Conf. on Mountain Meteorology,* Breckenridge, CO, Amer. Meteor. Soc., 212–215.

Ralph, F. M., P. J. Neiman, P. O. Persson, W. Neff, J. Miletta, L. Armi, and J. Bane, 1995: Observations of an orographically trapped disturbance along the California coast on 10–11 June 1994. *Proc. of the Seventh Conf. on Mountain Meteorology,* Breckenridge, CO, Amer. Meteor. Soc., 204–211.

Reason, C., and D. Steyn, 1990: Coastally trapped disturbances in the lower atmosphere: Dynamic commonalities and geographic diversity. *Prog. Phys. Geogr.*, **14,** 178–198.

——, and ——, 1992: The dynamics of coastally trapped mesoscale ridges in the lower atmosphere. *J. Atmos. Sci.*, **49,** 1677–1692.

Rogerson, A. M., and R. M. Samelson, 1995: Synoptic forcing of coastal-trapped disturbances in the marine atmospheric boundary layer. *J. Atmos. Sci.*, **52,** 2025–2040.

Thomson, R. E., 1970: On the generation of Kelvin-type waves by atmospheric disturbances. *J. Fluid Mech.*, **42,** 657–670.